Adsorption (2009) 15: 138–144
DOI 10.1007/s10450-009-9164-y

A simple method to ordered mesoporous carbons containing nickel nanoparticles

Xiqing Wang · Sheng Dai

Published online: 20 March 2009

Abstract A series of ordered mesoporous carbons containing magnetic Ni nanoparticles (Ni-OMCs) with a variety of Ni loadings was made by a simple one-pot synthetic procedure through carbonization of phenolic resin-Pluronic block copolymer composites containing various amount of nickel nitrate. Such composite materials were characterized by N_2 sorption, XRD, and STEM. Ni-OMCs exhibited high BET surface area, uniform pore size, and large pore volume without obvious pore blockage with a Ni loading as high as 15 wt%. Ni nanoparticles were crystalline with a face-center-cubic phase and observed mainly in the carbon matrix and on the outer surface as well. The average particle size of Ni nanoparticles was dependent on the preparation (carbonization) temperature and Ni loading; the higher the temperature was used and the more the Ni was incorporated, the larger the Ni nanoparticles were observed. One of the applications of Ni-OMCs was demonstrated as magnetically separable adsorbents.

Keywords Ordered mesoporous carbon · Magnetic · Adsorbent · Nickel · Synthesis

1 Introduction

Ordered mesoporous carbons (OMCs) have recently attracted much attention because of their structural regularity, chemical and thermal stabilities, and electrical conductivity (Liang et al. 2008). Incorporation of magnetic metal or metal oxide nanoparticles into OMCs without the blockage of mesoporosity is of great interest since it enables an alternative and simple separation of OMCs by means of an external magnetic field. Therefore, such composite materials are potentially useful as magnetically separable catalysts (Lee et al. 2005b), catalyst supports (Lu et al. 2004; Tian et al. 2007), and adsorbents (Cao et al. 2007b).

OMCs containing magnetic nanoparticles have so far been prepared by two general methods. The first method is to deposit or load magnetic nanoparticles on the pre-synthesized OMCs, which are prepared using ordered mesoporous silicas as the hard templates (Cao et al. 2007b; Lee et al. 2005b; Lu et al. 2004; Tian et al. 2007). For example, Lu et al. fabricated magnetic CMK-3 by depositing Co nanoparticles on the outer surface of a carbon/SBA-15 composite with coating of a thin carbon layer on Co nanoparticles to anchor them on the surface of CMK-3 and to prevent dissolution by HF. This method could be simplified by impregnation of a solution of iron salt or nickel salt into the pores of C/silica composites or OMCs, followed by the reduction of iron or nickel salt into magnetic Fe_3O_4 (Lee et al. 2005b; Tian et al. 2007) or Ni nanoparticles (Cao et al. 2007b), respectively. In the second method, ordered mesoporous silicas were pre-loaded with magnetic nanoparticles before filling the carbon precursor (Holmes et al. 2005), or were impregnated with both the carbon precursor and metal salts. In the latter case, the reduction of metal salts into magnetic nanoparticles occurred simultaneously with carbonization (Dong et al. 2007; Lee et al. 2005a; Park et al. 2006). However, these synthetic routes consist of multiple steps and require careful control of synthesis conditions. Therefore, a simple approach to magnetic OMCs is highly desirable.

Dedicated to Professor Mietek Jaroniec on the occasion of his 60th birthday.

X. Wang · S. Dai (✉)
Chemical Sciences Division, Oak Ridge National Laboratory, Oak Ridge, Tennessee 37831-6201, USA
e-mail: dais@ornl.gov

Recently, we and several other groups have developed a soft-templating method for the preparation of OMCs by self-assembly of phenolic resins and block copolymers (Liang and Dai 2006; Liang et al. 2004; Liu et al. 2007; Meng et al. 2005; Tanaka et al. 2005; Wang et al. 2008b; Zhang et al. 2005). In the present work, we describe a facile one-pot synthesis of OMCs containing magnetic Ni nanoparticles (Ni-OMCs) based on the soft-templating method. Such functional OMCs have been demonstrated to be magnetically separable adsorbents.

2 Experimental

2.1 Synthesis of OMCs containing Ni nanoparticles (Ni-OMCs)

Ni-OMCs were prepared by carbonization of polymeric composites, which were obtained by self-assembly of *in situ* formed phenolic resin and Pluronic block copolymer under acidic conditions (Liang and Dai 2006; Wang et al. 2008b), containing different amount of nickel nitrate. The polymeric composites could be made in a wide range of compositions (Wang et al. 2008b). In a typical synthesis, 2.2 g of resorcinol and 2.2 g of F127 ($EO_{106}PO_{70}EO_{106}$, Aldrich) were dissolved in 18.0 mL of a mixed solution of HCl-EtOH-H_2O (mass ratio: 32 concentrated HCl:100 EtOH:90 H_2O). To this solution, 2.6 g of formaldehyde (37%) was then added. After stirring for about 16 min at room temperature, the clear mixture turned turbid, indicating the formation of RF-F127 nanocomposite and a phase separation. The polymer-rich gel phase (Liang and Dai 2006) was collected in the bottom of the centrifuge tube by centrifugation at 9500 rpm for 4 min after the mixture was stirred for 40 min. The gel phase was then re-dissolved in 3.6 g of ethanolic solution of nickel nitrate ($Ni(NO_3)_2{\cdot}6H_2O$, 5 wt%). The mixture was loaded on a petri dish, air dried overnight, and then cured in an oven at 60 °C and 100 °C for 24 h each. Carbonization was carried out under N_2 atmosphere at 400 °C for 2 h with a heating rate of 1 °C/min, which was followed by further treatment at 850 °C for 3 h with a heating rate of 5 °C/min. The Ni wt% in the resulting Ni-OMC composite was calculated to be ca. 5% and the carbon material was denoted as Ni-C-ORNL-1-5%. By the same way, Ni-OMC composites containing various amounts of Ni were prepared and denoted as Ni-C-ORNL-1-10% and Ni-C-ORNL-1-15%. For comparison, C-ORNL-1 without Ni was also made.

2.2 Characterization

N_2 sorption analysis was performed on a Micromeritics Gemini analyzer at −196 °C (77 K). Prior to measurement, the sample was dried in a vacuum oven at 120 °C overnight. The specific surface area was calculated using the BET method from the nitrogen adsorption data in the relative range (P/P_0) of 0.06–0.30. The total pore volume was determined from the amount of N_2 uptake at $P/P_0 = 0.95$. The micropore volume was calculated from the intercept of the *V*–*t* plot, where the *t* values were calculated as a function of the relative pressure using the de Bore equation, $t/\text{Å} = [13.99/(\log(P_0/P) + 0.0340)]^{1/2}$. The pore size distribution (PSD) plot was derived from the adsorption branch of the isotherm based on the Barrett-Joyner-Halenda (BJH) model. XRD patterns were recorded on a Siemens D5005 diffractometer operating at 40 kV and 40 mA. Both SEM and TEM images were taken on a Hitachi HD-2000 STEM microscope operating at 200 kV under SE and TE modes, respectively.

2.3 Adsorption test

Ni-C-ORNL-1-10% (10 mg) and 10 mL of aqueous solution of Rhodamine B with various concentrations (0.05–0.2 mg/mL) were mixed and shaken at room temperature for 2 h. The dye loaded Ni-C-ORNL-1-10% was separated by an external magnet or by centrifugation. The concentrations of Rhodamine B remained in the solutions were determined spectrophotometrically by measuring the UV absorbance at 554 nm using a Cary 5000 UV-Vis-NIR spectrophotometer (Varian Inc.). The amounts of Rhodamine B adsorbed by Ni-C-ORNL-1-10% were calculated by the difference of concentrations before and after adsorption.

3 Results and discussion

Figure 1 shows the small-angle XRD patterns of C-ORNL-1 and Ni-OMCs. C-ORNL-1 displays three well-resolved peaks, which are indexed to the 100, 110, and 200 reflections of the 2D hexagonal symmetry (*p6mm*), suggesting

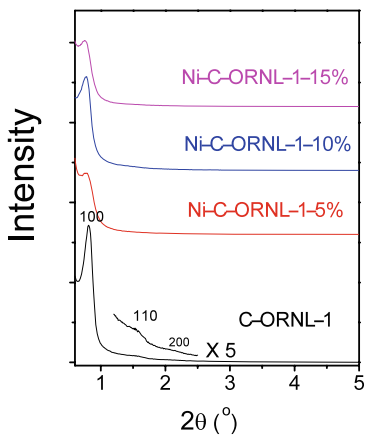

Fig. 1 Small-angle XRD patterns of C-ORNL-1 and Ni-OMCs

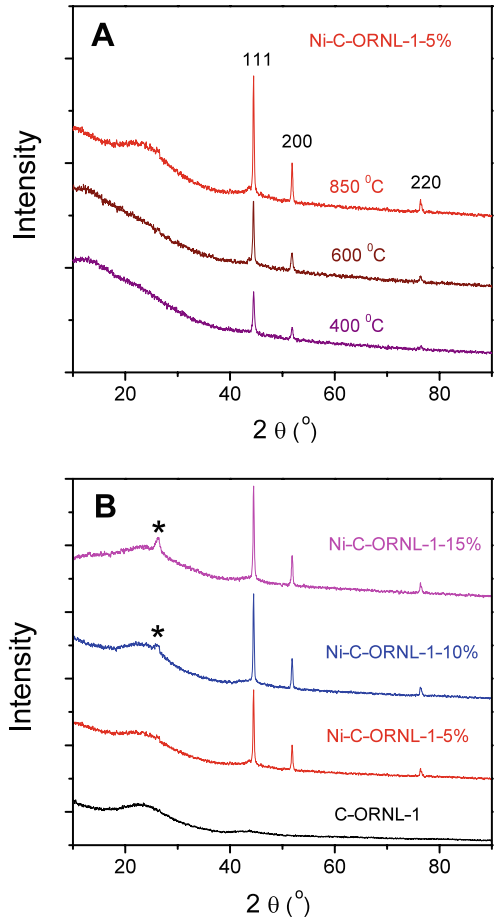

Fig. 2 Wide-angle XRD patterns of Ni-C-ORNL-1-5% (**A**) heated at elevated temperatures, from 400 to 850 °C, and of C-ORNL-1 and Ni-OMCs (**B**) prepared at 850 °C. The peaks arose from graphitic carbon are marked by *asterisk*

an ordered mesostructure. However, all of Ni-OMCs samples show only the 100 reflection and the intensities of this peak are weaker than that of C-ORNL-1, indicating a less ordered hexagonal mesostructure than that of C-ORNL-1.

The wide-angle XRD pattern of Ni-C-ORNL-1-5% thermally treated at 400 °C (Fig. 2a) shows three peaks at 44.5°, 51.8°, and 76.4°, revealing the characteristics of face-centered cubic (fcc) nickel, while no nickel carbide or nickel oxide is detected. It has been shown that carbonization of sucrose in the presence of nickel salt with SBA-15 resulted in CMK-3 containing NiO nanoparticles rather than Ni nanoparticles embedded into carbon framework (Cao et al. 2007a; Li et al. 2006), although thermodynamically NiO nanoparticles could be reduced into Ni by carbon. Only a small fraction of NiO could be reduced to Ni when the carbonization temperature was increased to 1000 °C, which was probably due to the passivation and stabilization of NiO nanoparticles via reducing the surface energy of NiO by the carbon framework (Li et al. 2006). The exact reason still remained unclear. Therefore, OMCs containing Ni nanoparticles were prepared through H_2 reduction of NiO-OMCs composites (Huwe and Fröba 2007) or impregnation of CMK-3 with nickel salt followed by carbonization in an inert gas atmosphere (Cao et al. 2007b). On the contrary to the above results, in the current study, the formation of Ni nanoparticles was observed when the polymeric gels containing nickel nitrate were heated even at 400 °C in an inert gas atmosphere. The formation of nickel metal nanoparticles was realized through reduction of nickel salt by probably CO, H_2, or other reducing species, which were generated during decomposition of block copolymer and pyrolysis of phenolic resin (Wang et al. 2008b). Increasing the carbonization temperature resulted in an increase in the intensities of Ni XRD peaks (Fig. 2a), which was likely attributed to the aggregation of Ni nanoparticles. As expected, increasing the Ni-loading in the Ni-OMCs also led to an increase in the intensities of Ni XRD peaks (Fig. 2b). In addition, an individual diffraction peak of graphitic carbon at 2θ around 26°(002) was observed for the Ni-OMCs with high loading of Ni (i.e., Ni-C-ORNL-1-10% and Ni-C-ORNL-1-15%). According to previous studies (Meng et al. 2005; Wang et al. 2008b; Zhang et al. 2005), the treatment of the Pluronic block copolymer-phenolic resin composite at 400 °C in an inert gas atmosphere led to the formation of a mesoporous polymer. Therefore, one of the unique features of the method described here is to allow the preparation of ordered mesoporous polymers containing Ni nanoparticles as well as other metal and metal oxide nanoparticles.

Figure 3 shows the N_2 sorption isotherms and the BJH pore size distribution plots of C-ORNL-1 and Ni-OMCs. All of these materials exhibit typical type IV isotherms with a steep condensation step at relative pressures (P/P_0) of 0.5–0.75 and a type H1 hysteresis loop, indicating the presence of uniform mesoporosity. As listed in Table 1, Ni-C-ORNL-1-5% exhibits a comparable BET surface area (660 m^2/g) and total pore volume (0.68 cm^3/g) to those of C-ORNL-1. However, there is a decrease in BET surface area and total pore volume as the loading of Ni increases in Ni-OMCs, which is likely due to the increased mass as a result of incorporating Ni nanoparticles and/or the blockage of mesopores by Ni nanoparticles. Notably, Ni-C-ORNL-1-15% shows a tardy desorption branch, clearly indicating a blockage of mesopores. Further increasing the loading of Ni in the polymeric gels leads to gradual degradation of the ordered mesostructures of the Ni-C composites (data not shown).

The dispersion and sizes of Ni nanoparticles within the carbon materials were investigated using TEM. Figure 4 shows the typical TEM images of Ni-C-ORNL-1-5% prepared at elevated temperatures. The dark spots with diameters ranging from 30 nm to 200 nm are Ni nanoparticles and the stripe patterns are assigned to the lattice fringes of the hexagonal mesostructure. The distribution of Ni nanoparticles is approximately homogeneous and the Ni particle sizes

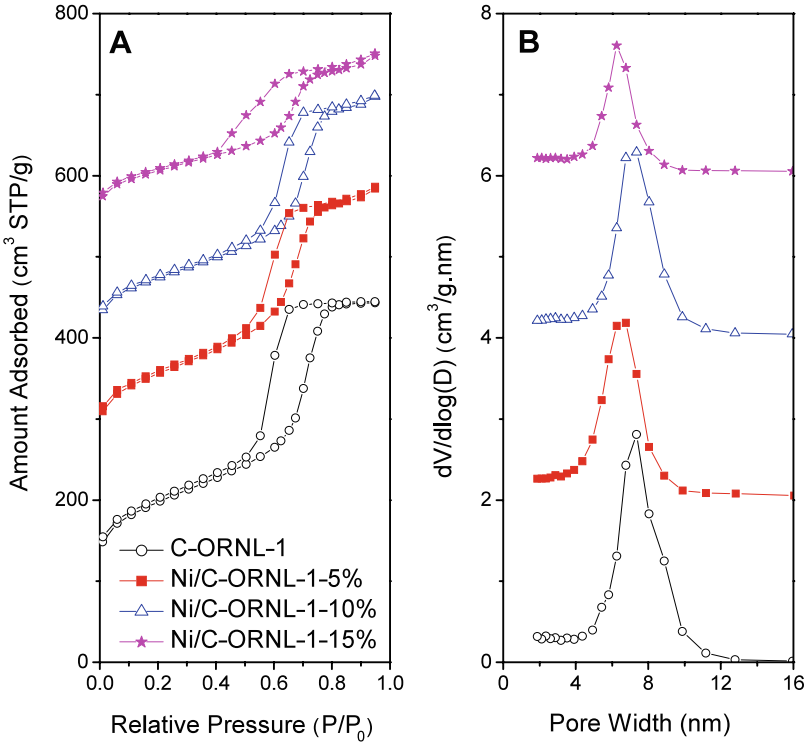

Fig. 3 N_2 sorption isotherms (**A**) and BJH pore size distribution plots (**B**) of C-ORNL-1 (○), Ni-C-ORNL-1-5% (■), Ni-C-ORNL-1-10% (△), and Ni-C-ORNL-1-15% (★). For clarity, the isotherms (**A**) of Ni-C-ORNL-1-5%, Ni-C-ORNL-1-10%, and Ni-C-ORNL-1-15% are vertically upset by 150, 300, and 450 cm^3 STP/g, respectively. The PSD plots (**B**) of Ni-C-ORNL-1-5%, Ni-C-ORNL-1-10%, and Ni-C-ORNL-1-15% are vertically upset by 2, 4, and 6 $cm^3/g{\cdot}nm$, respectively

Table 1 Structural properties of C-ORNL-1 and Ni-OMCs[a]

Material	$S_{BET}(m^2/g)$	$V_t(cm^3/g)$	$V_m(cm^3/g)$	w(nm)
C-ORNL-1	641	0.69	0.19	7.4
Ni-C-ORNL-1-5%	660	0.68	0.21	6.8
Ni-C-ORNL-1-10%	561	0.62	0.17	7.4
Ni-C-ORNL-1-15%	497	0.46	0.17	6.3

[a] S_{BET}: BET surface area; V_t: total pore volume; V_m: micropore volume; w: BJH pore size

are quite uniform for Ni-C-ORNL-1-5% heated at 400 °C. The Ni nanoparticles are mostly in quasi-spherical shape although some other morphologies are also observed. Interestingly, it is clearly seen that the Ni particle sizes increase gradually as the preparation temperature is increased. In addition, the Ni particle size distribution becomes broader for the samples prepared at higher temperatures than the one prepared at 400 °C. The histograms for the particle size distribution are plotted by counting more than 100 Ni particles from the TEM images, and the average particle sizes are estimated to be 48 nm at 400 °C, 83 nm at 600 °C, and 101 nm at 850 °C, respectively. The results indicate that smaller Ni nanoparticles are tended to aggregate with neighbors to form bigger ones at elevated temperatures, as revealed in Fig. 4B, in which the aggregation of two particles is marked by an arrow. The dependence of metal nanoparticle sizes in the carbon matrix on the preparation temperature has also been found by others (Park et al. 2006).

The average size of Ni nanoparticles increases as the Ni loading in Ni-OMCs is increased, reaching a value of 114 ± 34 nm for the sample Ni-C-ORNL-1-10% (Figs. 5A, 5B, and 5C). After carefully comparing the SEM and TEM images of Ni-C-ORNL-1-10% on the same area, one can find that a small portion of Ni nanoparticles is decorated on the outer surface of the Ni-C composite, as indicated by circles in Figs. 5A and 5B. This phenomenon is hardly observed for Ni-C-ORNL-1-5%. Moreover, the 2D hexagonal mesostructure of Ni-C-ORNL-1-10% is clearly observed (Fig. 5C). In the case of Ni-C-ORNL-1-15%, the particle size distribution of Ni nanoparticles is very broad, ranging from 30 nm to hundreds of nm. A comparison of the SEM and TEM images of Ni-C-ORNL-1-15% on the same area reveals that a significant portion of Ni nanoparticles is located on the outer surface and formed as very large aggregates, such as those shown by circles in Figs. 5D and 5E. The formation of large Ni aggregates on the outer surface decreases the content of Ni inside the carbon particles, and

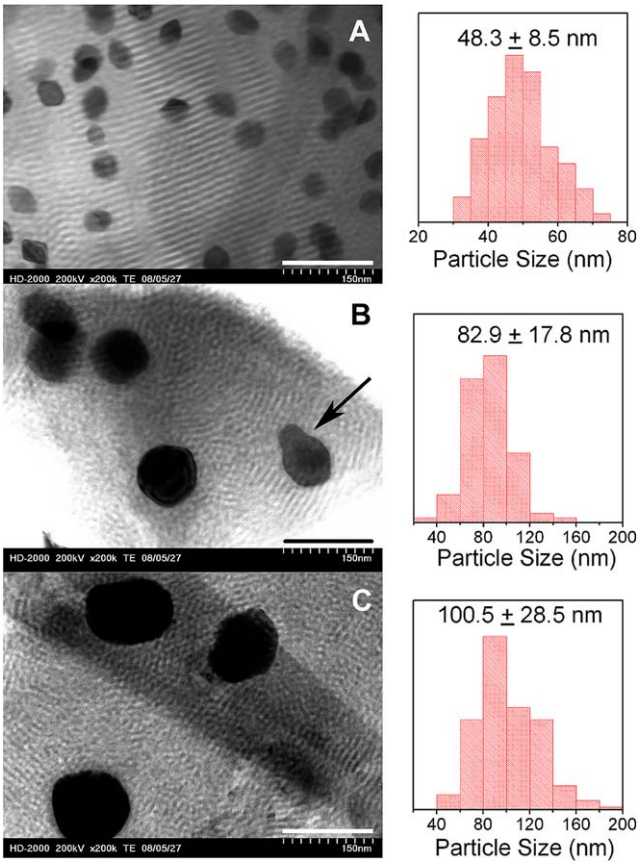

Fig. 4 Typical TEM images of Ni-C-ORNL-1-5% heated at different temperatures: (**A**) 400 °C, (**B**) 600 °C, and (**C**) 850 °C. The scale bar is 150 nm. The histograms show particle size distributions of Ni nanoparticles, as estimated from the TEM images

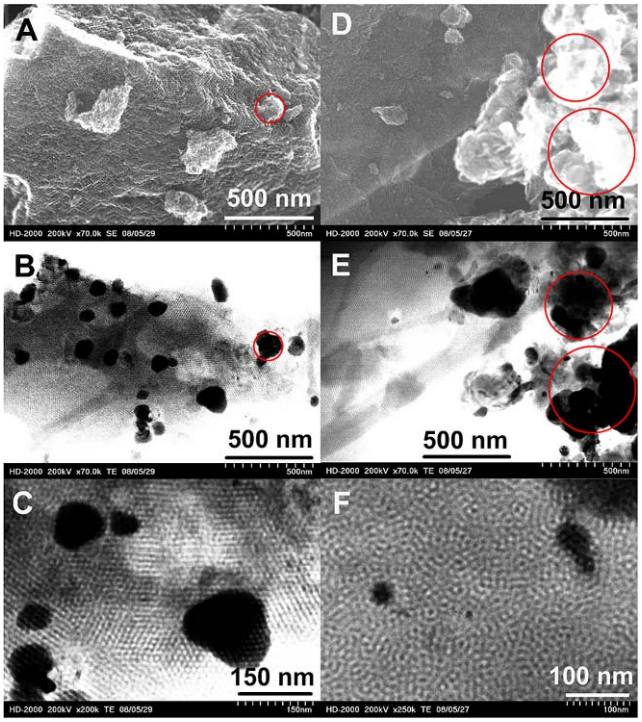

Fig. 5 Typical SEM and TEM images of Ni-C-ORNL-1-10% (**A**, **B**, and **C**) and Ni-C-ORNL-1-15% (**D**, **E**, **F**). Images **A** and **B** of Ni-C-ORNL-1-10%, **D** and **E** of Ni-C-ORNL-1-15% are taken on the same areas under the SE and TE mode, respectively

thus probably it is the reason for the observation of considerable amounts of small Ni nanoparticles (e.g. 30 nm). Such large Ni aggregates on the outer surface may also limit the diffusion of guest molecules into and out from mesopores, as suggested by the N_2 desorption behavior (Fig. 3A). In addition, a wormy mesostructure (Fig. 5F) as well as 2D hexagonal mesostructure (Fig. 5E) is observed for Ni-C-ORNL-1-15%, which is in agreement with its broad XRD peak at 2θ around 0.8° with low intensity (Fig. 1).

OMCs containing Ni nanoparticles are expected to be good magnetically separable catalysts, catalytic supports, and adsorbents. One of these applications was demonstrated by using Ni-C-ORNL-1-10% as an adsorbent for the adsorption of Rhodamine B from aqueous solution. Figure 6A shows an aqueous solution of Rhodamine B (0.1 mg/mL). After the addition of Ni-C-ORNL-1-10%, the solution changed its color from red to colorless within minutes, indicating a quick uptake of Rhodamine B by Ni-C-ORNL-1-10%. The dye loaded Ni-C-ORNL-1-10% could be easily separated from the solution by an external magnet, as shown in Fig. 6A. The colorless solution could be decanted off and the adsorbent could be recovered by washing with ethanol. The adsorption capacity of Rhodamine B on Ni-C-ORNL-1-10% is determined to be 166 mg/g (Fig. 6B). It should be noted that the adsorption capacity of Rhodamine B on carbon materials is dependent on the structural properties of carbon materials, pH, and temperature (Arivoli and Thenkuzhali 2008; Guo et al. 2005) and is not the focus of the current study.

4 Conclusion

Ordered mesoporous carbons with Ni nanoparticles (Ni-OMCs) have been prepared using a simple one-pot synthetic procedure, which employs the carbonization of phenolic resin-Pluronic block copolymer composites containing nickel nitrate in an inert gas atmosphere. Ni-OMCs exhibit uniform PSDs for mesopores, high BET surface area, and large pore volume. Ni nanoparticles, ranging from tens of nm to hundreds of nm, are found to be embedded in the carbon framework and also located on the carbon outer surface. The application of such materials as magnetically separable adsorbents for removing Rhodamine B from aqueous solution was demonstrated. Such magnetic composites could also be used as adsorbents for other molecules, such as large biomolecules. Upon functionalization of carbon surface (Li and Dai 2005; Li et al. 2005; Wang et al. 2007, 2008a) or

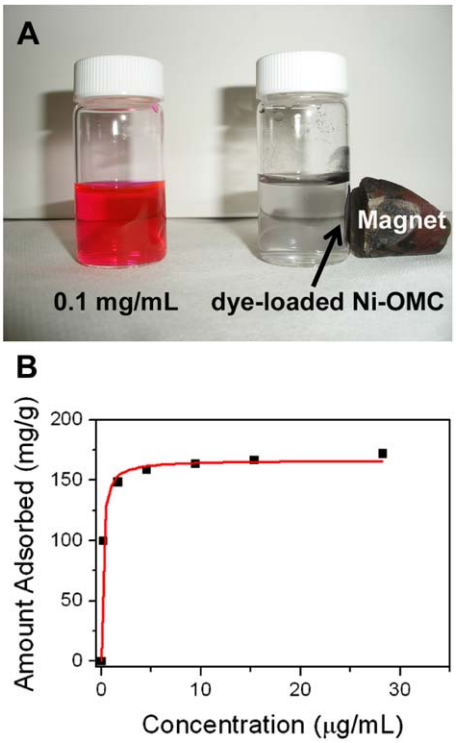

Fig. 6 (**A**) A digital graph shows an aqueous solution of Rhodamine B (0.1 mg/mL, *left*) and separation of dye loaded Ni-OMC by a magnet (*right*). (**B**) Adsorption isotherm of Rhodamine B on Ni-C-ORNL-1-10% as a function of concentration at equilibrium

loading of nano catalysts into the carbon matrix (Lu et al. 2004; Tian et al. 2007), Ni-OMCs hold great promise as magnetically recoverable catalysts or catalyst supports. The method described here could be applied to prepare ordered mesoporous carbons containing other metal and metal oxide nanoparticles.

Acknowledgements This work was conducted at the Oak Ridge National Laboratory and supported by the Division of Chemical Sciences, Office of Basic Energy Sciences, U.S. Department of Energy, under contract No. DE-AC05-00OR22725 with UT-Battelle, LLC. This research was supported in part by an appointment for X.W. to the Oak Ridge National Laboratory Postdoctoral Research Associates Program, administered jointly by the Oak Ridge Institute for Science and Education and Oak Ridge National Laboratory.

References

Arivoli, S., Thenkuzhali, M.: Kinetic, mechanistic, thermodynamic and equilibrium studies on the adsorption of rhodamine B by acid activated low cost carbon. E-J. Chem. **5**, 187–200 (2008)

Cao, Y.L., Cao, J.M., Zheng, M.B., Liu, J.S., Ji, G.B.: Synthesis, characterization, and electrochemical properties of ordered mesoporous carbons containing nickel oxide nanoparticles using sucrose and nickel acetate in a silica template. J. Solid State Chem. **180**, 792–798 (2007a)

Cao, Y.L., Cao, J.M., Zheng, M.B., Liu, J.S., Ji, G.B., Ji, H.M.: Facile fabrication of magnetic nanocomposites of ordered mesoporous carbon decorated with nickel nanoparticles. J. Nanosci. Nanotechnol. **7**, 504–509 (2007b)

Dong, X.P., Chen, H.R., Zhao, W.R., Li, X., Shi, J.L.: Synthesis and magnetic properties of mesostructured γ–Fe_2O_3/carbon composites by a co-casting method. Chem. Mater. **19**, 3484–3490 (2007)

Guo, Y.P., Zhao, J.Z., Zhang, H., Yang, S.F., Qi, J.R., Wang, Z.C., Xu, H.D.: Use of rice husk-based porous carbon for adsorption of Rhodamine B from aqueous solutions. Dyes Pigments **66**, 123–128 (2005)

Holmes, S.M., Foran, P., Roberts, E.P.L., Newton, J.M.: Encapsulation of metal particles within the wall structure of mesoporous carbons. Chem. Commun. 1912–1913 (2005)

Huwe, H., Fröba, M.: Synthesis and characterization of transition metal and metal oxide nanoparticles inside mesoporous carbon CMK-3. Carbon **45**, 304–314 (2007)

Lee, J., Jin, S., Hwang, Y., Park, J.-G., Park, H.M., Hyeon, T.: Simple synthesis of mesoporous carbon with magnetic nanoparticles embedded in carbon rods. Carbon **43**, 2536–2543 (2005a)

Lee, J., Lee, D., Oh, E., Kim, J., Kim, Y.-P., Jin, S., Kim, H.-S., Hwang, Y., Kwak, J.H., Park, J.-G., Shin, C.-H., Kim, J., Hyeon, T.: Preparation of a magnetically switchable bioelectrocatalytic system employing cross-linked enzyme aggregates in magnetic mesocellular carbon foam. Angew. Chem., Int. Ed. **44**, 7427–7432 (2005b)

Li, H.F., Zhu, S.M., Xi, H.A., Wang, R.D.: Nickel oxide nanocrystallities within the wall of ordered mesoporous carbon CMK-3: synthesis and characterization. Microporous Mesoporous Mater. **89**, 196–203 (2006)

Li, Z.J., Dai, S.: Surface functionalization and pore size manipulation for carbons of ordered structure. Chem. Mater. **17**, 1717–1721 (2005)

Li, Z.J., Yan, W.F., Dai, S.: Surface functionalization of ordered mesoporous carbons—a comparative study. Langmuir **21**, 11999–12006 (2005)

Liang, C.D., Dai, S.: Synthesis of mesoporous carbon materials via enhanced hydrogen-bonding interaction. J. Am. Chem. Soc. **128**, 5316–5317 (2006)

Liang, C.D., Hong, K.L., Guiochon, G.A., Mays, J.W., Dai, S.: Synthesis of a large-scale highly ordered porous carbon film by self-assembly of block copolymers. Angew. Chem., Int. Ed. **43**, 5785–5789 (2004)

Liang, C.D., Li, Z.J., Dai, S.: Mesoporous carbon materials: synthesis and modification. Angew. Chem., Int. Ed. **47**, 3696–3717 (2008)

Liu, C.Y., Li, L.X., Song, H.H., Chen, X.H.: Facile synthesis of ordered mesoporous carbons from F108/resorcinol-formaldehyde composites obtained in basic media. Chem. Commun. 757–759 (2007)

Lu, A.-H., Schmidt, W., Matoussevitch, N., Bonnemann, H., Spliethoff, B., Tesche, B., Bill, E., Kiefer, W., Schüth, F.: Nanoengineering of a magnetically separable hydrogenation catalyst. Angew. Chem., Int. Ed. **43**, 4303–4306 (2004)

Meng, Y., Gu, D., Zhang, F.Q., Shi, Y.F., Yang, H.F., Li, Z., Yu, C.Z., Tu, B., Zhao, D.Y.: Ordered mesoporous polymers and homologous carbon frameworks: amphiphilic surfactant templating and direct transformation. Angew. Chem., Int. Ed. **44**, 7053–7059 (2005)

Park, I.-S., Choi, M., Kim, T.-W., Ryoo, R.: Synthesis of magnetically separable ordered mesoporous carbons using furfuryl alcohol and cobalt nitrate in a silica template. J. Mater. Chem. **16**, 3409–3416 (2006)

Tanaka, S., Nishiyama, N., Egashira, Y., Ueyama, K.: Synthesis of ordered mesoporous carbons with channel structure from an organic-organic nanocomposite. Chem. Commun. 2125–2127 (2005)

Tian, Y., Li, G.-D., Gao, Q., Xiu, Y., Li, X.-H., Chen, J.-S.: A facile route to mesoporous carbon catalyst support modified with magnetic nanoparticles. Chem. Lett. **36**, 422–423 (2007)

Wang, X.Q., Liu, R., Waje, M.M., Chen, Z.W., Yan, Y.S., Bozhilov, K.N., Feng, P.Y.: Sulfonated ordered mesoporous carbon as a stable and highly active protonic acid catalyst. Chem. Mater. **19**, 2395–2397 (2007)

Wang, X.Q., Jiang, D.-E., Dai, S.: Surface modification of ordered mesoporous carbons via 1,3-dipolar cycloaddition of azomethine ylides. Chem. Mater. **20**, 4800–4802 (2008a)

Wang, X.Q., Liang, C.D., Dai, S.: Facile synthesis of ordered mesoporous carbons with high thermal stability by self-assembly of resorcinol-formaldehyde and block copolymers under highly acidic conditions. Langmuir **24**, 7500–7505 (2008b)

Zhang, F.Q., Meng, Y., Gu, D., Yan, Y., Yu, C.Z., Tu, B., Zhao, D.Y.: A facile aqueous route to synthesize highly ordered mesoporous polymers and carbon frameworks with *Ia-3d* bicontinuous cubic structure. J. Am. Chem. Soc. **127**, 13508–13509 (2005)